International Journal of
Plasma Environmental Science and Technology

Regular Paper DOI: 10.34343/ijpest.2020.14.e01008

The effects of pulse frequency on chemical species formation in a nanosecond pulsed plasma gas-liquid film reactor

Robert J. Wandell[1], Stefan Bresch [2], Huihui Wang[1], Vaclav Babicky[2], Petre Lukes[2], Bruce R. Locke[1,*]

[1] Department of Chemical and Biomedical Engineering, FAMU-FSU College of Engineering, Florida State University, Tallahassee FL, United States
[2] Institute of Plasma Physics of the Czech Academy of Sciences, Pulse Plasma Systems Department, Prague 8, Czech Republic

* Corresponding author: locke@eng.famu.fsu.edu (Bruce R. Locke)

Received: 24 January 2020
Revised: 1 April 2020
Accepted: 2 April 2020
Published online: 7 April 2020

Abstract

The influence of pulse frequency (1−60 kHz) in a nanosecond filamentary discharge propagating along a flowing liquid water film was assessed with regards to the formation of chemical species with argon and helium carrier gasses. The production rate and energy yield for H_2O_2 and H_2 were measured for both carrier gases, and O_2 formation was determined for helium. The effect of pulse frequency on the energy dissipated per pulse as well as electron density was also investigated. The results indicate that the energy yield for H_2O_2 decreases with increasing pulse frequency while the energy yields of H_2 and O_2 remain relatively unaffected. It is proposed that the difference in the trends of the liquid versus gas phase products can be attributed to the significantly longer residence time of the liquid phase allowing for more degradation of formed hydrogen peroxide before it is able exit the reactor.

Keywords: Non-thermal plasma, nanosecond discharge, hydrogen peroxide, pulse frequency, filamentary discharge, wet plasma.

1. Introduction

There is significant interest in the design and development of chemical reactors that incorporate electrical discharge plasma which simultaneously contacts gas and liquid-water phases for applications in environmental, chemical, agricultural, and biomedical engineering and science [1−4]. In systems where the gas phase carrier is a noble gas, e.g. helium or argon, which contacts liquid water, the major stable molecular products are typically H_2O_2, usually measured in the liquid exiting the reactor [5], as well as H_2 and O_2, mostly found in the gas phase exiting the reactor (although less frequently reported) [6]. Previous work in our group has focused on the analysis of a tubular gas-liquid flowing film plasma reactor where the plasma propagates along the interface between a flowing gas and a flowing liquid film [7]. The formation of H_2O_2 [8], the gas-liquid hydrodynamics [8], the degradation of various organic compounds [9, 10], the effects of carrier gas on H_2O_2 formation [11], the formation of hydroxyl radicals [12], and the role of two different power delivery means, e.g. nano-second vs microsecond pulses [13], have been reported. Combined modeling and experimental studies suggested that the energy yield and production rates of H_2O_2 are limited by degradation reactions [11]. Since one possible method to increase the production rate of a desired chemical species such as, for example, H_2O_2, in such a system is to increase the frequency of the plasma discharge, the present work focuses on the role of pulse frequency on the production of H_2O_2, H_2, and O_2 in this gas-liquid plasma discharge reactor with a nanosecond pulsed power supply. While H_2O_2 has often been the focus of previous work, primarily due to the ease of measurement, key insights into the gas-liquid plasma chemistry can be obtained through consideration of the formation of H_2 and O_2 [14], and of course these products can also be of inherent

importance for various applications. Since H_2 and O_2 are detected in the gas stream exiting the reactor and H_2O_2 is measured in the liquid stream exiting the reactor, the effects of pulse frequency on the relative formation of these species can provide information on the nature of degradation reactions taking place in the gas phase versus the liquid phase.

2. Experimental

A process schematic for the flowing film reactor system used in this study is provided in Fig. 1. With the exception of the power supply, this reactor system was nearly identical to our previous publications [8, 11, 15]. Deionized water was delivered to the system at a constant rate with a high-pressure syringe pump. The water stream combined with a high-pressure carrier gas stream before the mixture was fed into the inlet of the reactor through a stainless-steel capillary tube with a 0.25 mm inner diameter (I.D.). Upon entering the discharge region of the reactor, boxed in red in Fig. 1, the liquid coalesced on the reactor walls while the gas phase flowed through the central core of the tubular discharge region [8]. This created a flowing liquid film along the walls of the discharge region across which the plasma channels propagated. The plasma treated gas-liquid mixture exited the discharge region through a second stainless steel capillary tube, 1.0 mm I.D. For this work the liquid and gas flow rates were held constant at 2 mL min^{-1} and 0.5 L min^{-1}, respectively. Both argon and helium were used as carrier gasses.

The stainless-steel inlet and outlet capillaries also served as the plasma electrodes. A commercially available nanosecond high voltage (HV) pulse generator (Airity technologies, LLC) was utilized to generate the plasma discharge. Each high voltage nanosecond pulse sent to the reactor generated a single filamentary plasma channel in the discharge region as shown in Fig. 1, thus the frequency of the HV pulses was directly correlated to the frequency of the arcing events. The pulse frequency was modulated with a function generator, and a variable DC power supply was used to supply power to the HV pulse generator. The driver for the HV pulse generator was a variable DC power supply held constant at 100 Vdc.

Electrical diagnostics were performed with an oscilloscope (Tektronix, DPO 5204B) in conjunction with two HV probes (North Star, PVM−4) and current transformer (Pearson Electronics, 6585). The leads of the HV probes were connected across the stainless-steel inlet and outlet capillaries and the grounds of the probes were connected in order to measure the electric potential between the electrodes. The Rogowski coil was centered around the plasma reactor body to measure current flow through the discharge region. The energy per pulse was calculated by multiplying the voltage and current and integrating the resulting power over the time period of a single pulse [8, 11].

$$\text{Energy per pulse} = \int (V \times I) dt \quad (1)$$

V is instantaneous voltage, I is instantaneous current, and t is time. Total discharge power was calculated by multiplying the energy per pulse by the pulse frequency. Based on previous experimentation and published work with the same measurement techniques, the error in these measurements was less than 10%, which is the approximate size of the markers used in Figs. 3 and 4, thus the marker size can be used as an approximation of the error.

Time averaged optical emission spectroscopy (OES) was utilized to assess the electron density of the plasma channels (Avantes, AvaSpec-ULS3848; wavelength range: 600−700 nm). The plasma reactor body was constructed from a quartz block to eliminate optical interference. For these measurements, the optical fiber was positioned so its tip was flush against the quartz reactor body and oriented into the center of the discharge region. Stark broadening of the H_α peak at 656.3 nm using two-Voigt function was used for estimation of the electron density [11, 13, 16, 17]. These time averaged values can be viewed as estimates for the average election density and gas (plasma) temperature inside plasma channel depicted in Fig. 1.

After exiting the plasma reactor, the gas-liquid mixture was separated for independent analysis of the two phases. The H_2O_2concentration in the liquid phase was measured with the $TiSO_4$ colorimetric method using a UV-Vis spectrophotometer (Unicam Helios Gamma) [18]. The concentrations of hydrogen and oxygen in the gas phase exiting the reactor were determined by gas chromatography, Shimadzu GC-2010 Plus, equipped with barrier discharge ionization detector (BID-2010 Plus), helium carrier gas, and a Restek ShinCarbon ST Micropacked column (2 m × 1 mm I.D.). Oxygen concentrations could not be obtained when argon was used as the gas phase in the plasma system due to overlap of the oxygen signal with argon.

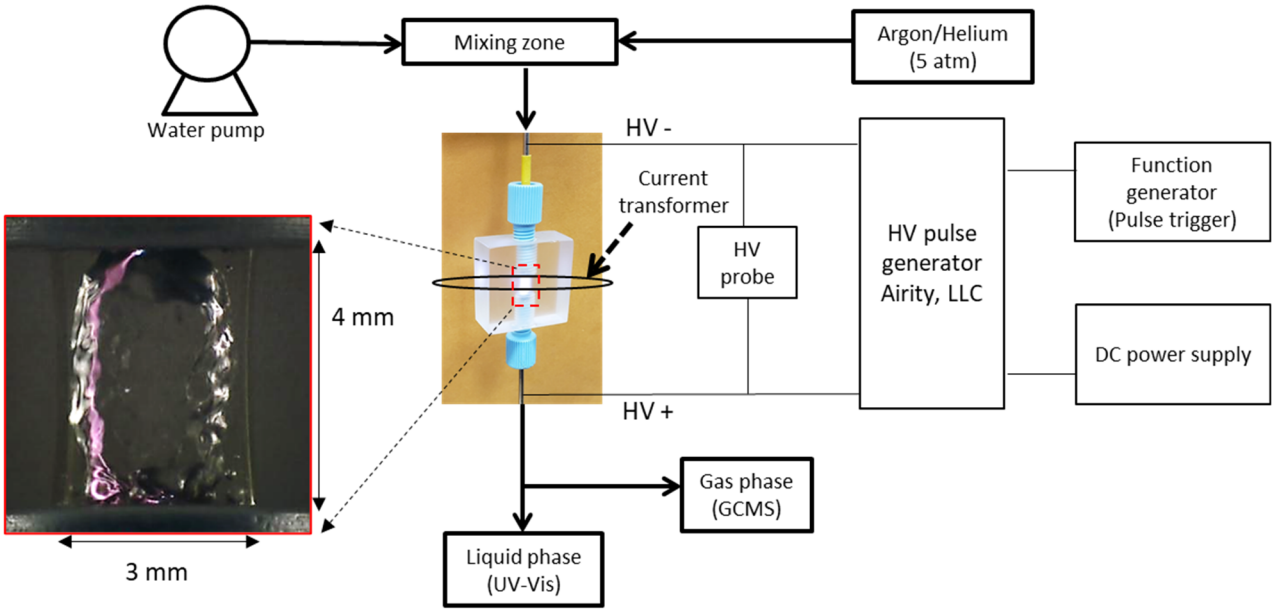

Fig.1. Process schematic of the experimental setup used in this work. The discharge region of the plasma is depicted in dotted red box. Photo insert taken at 1/8000 s exposure shows one plasma channel propagating along the gas/liquid interface.

3. Results and discussion

3.1 Electrical and plasma analysis

In Fig. 2, voltage and current waveforms are shown for both argon and helium carrier gasses at a 10 kHz pulse frequency. The rise rate of the voltage for the HV pulse generator used was approximately 0.04 kV ns^{-1} which is relatively slow compared to other nanopulsers. The rate of rise was independent of frequency and carrier gas. The breakdown voltage for argon occurred at 3800 V while the breakdown voltage for helium was significantly lower at 3000 V. This is consistent with our previous work with a different nanosecond power supply with a faster rate of rise, 0.25 kV ns^{-1}, as well as others [11, 19, 20]. When these breakdown values are compared to Paschen curves found in the literature, the values are lower than would be expected for a 4 mm point to plane discharge in pure gas (argon ≈ 10 kV and helium ≈ 6 kV). The reduced values found for this system can be explained by the high inhomogeneous nature of the discharge as well as the presence of the liquid film. The reduced breakdown of helium compared to argon is also consistent with the literature [21].

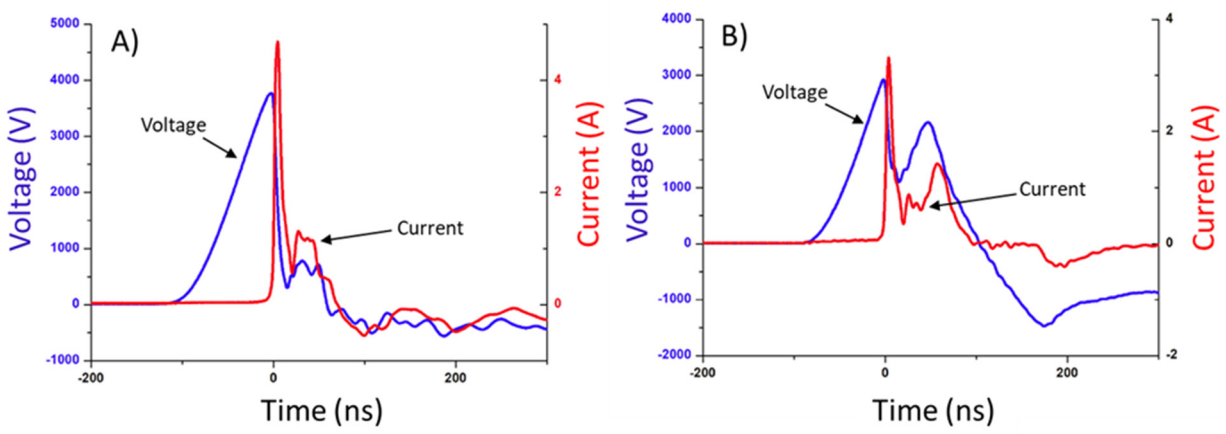

Fig. 2. Current and voltage waveforms for a single pulse for argon carrier gas (A) and helium (B) for 10 kHz pulse frequency.

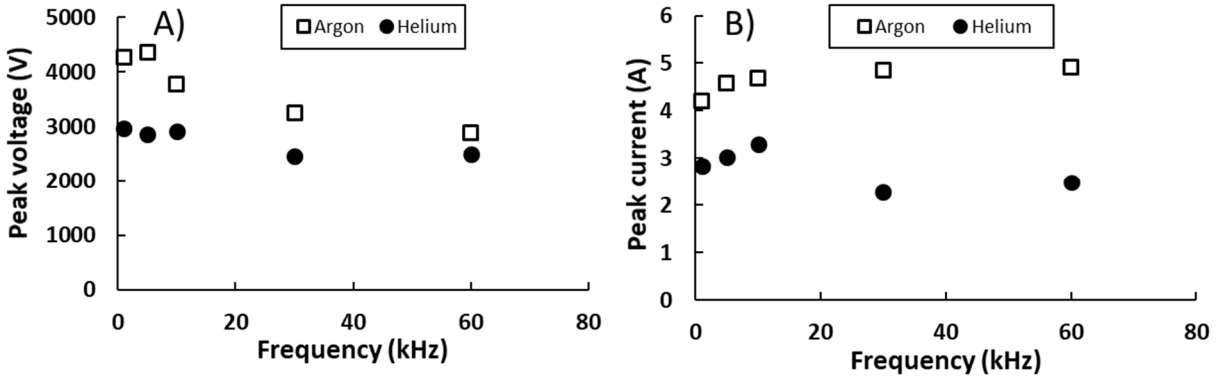

Fig. 3. Peak voltage and peak current as a function of pulse frequency for both argon and helium carrier gasses.

Fig. 3 (a) and 3 (b) show the peak voltage (breakdown voltage) and current as functions of pulse frequency for both argon and helium carrier gasses. The lower breakdown voltage for helium compared to argon is consistent across all pulse frequencies investigated. A decrease in breakdown voltage as the pulse frequency was increased was also observed for both gasses. For argon, the breakdown voltage dropped from 4300 V to 2900 V, a 32% decrease. For helium, the breakdown voltage dropped 17% from 3000 V to 2500 V. The decrease in breakdown voltage with increasing pulse frequency is likely due to excited molecules left over in the gas phase from the previous pulse. Due to the reduced ionization energy of these excited molecules, less energy, and thus a lower voltage potential, is required to induce electrical breakdown. The residence time for the gas was 2.5 ms [8] while the pulse period ranged from 1 ms at 1 kHz to 0.017 ms at 60 kHz. Because the timescale between pulses decreased with increasing pulse frequency while the gas residence time remained unchanged, there is a higher probability that these "left over" excided molecules will affect the next pulse at high frequency. We believe this phenomenon to be analogous to results found with nanosecond pulsed dry air discharges where it was dubbed an 'accumulation' or 'memory' effect [22]. This also implies that as pulse frequency increases, there is a higher likelyhood that successive plasma channels will follow the same path (appear in the same spatial location within the discharge region). With regards to peak current, there was no discernable trend or significant change with variation of pulse frequency.

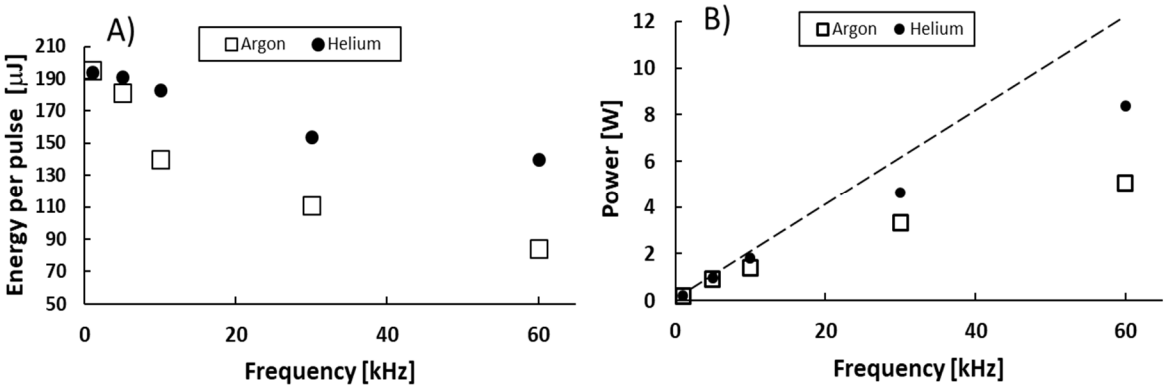

Fig. 4. Energy per pulse (A) and discharge power (B) as a function of pulse frequency for both argon and helium carrier gasses. Dashed line represents what would be expected if there were no change in energy per pulse with frequency.

The energy dissipated during a single pulse for argon and helium carrier gasses is plotted as a function of pulse frequency in Fig. 4 (a). For a 1 kHz pulse frequency, the energy dissipated for both argon and helium were within experimental error, 194 μJ. The energy per pulse decreased for both argon and helium as pulse frequency was increased. The decrease was more significant for argon, dropping to 84 μJ at 60 kHz, a 57% decrease. The energy per pulse for helium at 60 kHz was 140 μJ, a 28% decrease. This decrease can be attributed to the decrease in breakdown voltage with increasing pulse frequency. Fig. 4 (b) shows the change in total discharge power with pulse frequency. The dashed line in this figure represents what would be expected

if there were no change in energy per pulse with frequency and was generated by assuming a linear increase between 1 and 5 kHz and extrapolating to higher frequencies. Due to the decrease of energy per pulse with frequency, the total discharge power does not scale linearly with pulse frequency. This is clearly shown by the deviation of the experimental data from the dashed line.

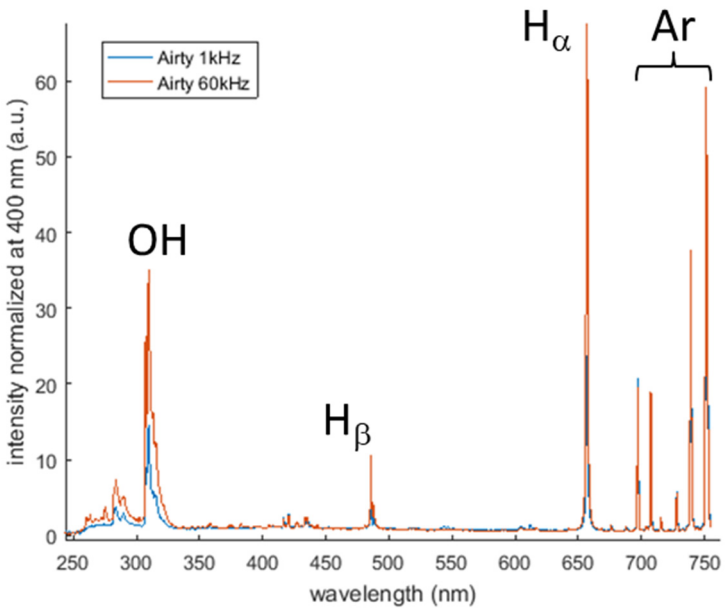

Fig. 5. Sample optical emission spectra from argon carrier gas at 1 kHz pulse frequency and 60 kHz pulse frequency.

Sample optical emission spectra for argon carrier gas are shown in Fig. 5 for 1 and 60 kHz pulse frequency. The large peak centered at 310 nm is indicative of ·OH emission while the peak at 656 nm is indicative of the Hα emission. Both of these bands increased in intensity when pulse frequency was increased. In a previous publication utilizing the same reactor configuration with a slightly different power supply, the background gas temperature was estimated for both argon and helium carrier gasses using a two-temperature fitting method of the ·OH emission at 310 nm. In that study the gas temperature was found to be 800 ± 100 K for argon and 350 ± 50 K for helium [11]. This difference was attributed to the helium discharge being more diffuse (larger plasma volume) due to the helium having a higher ion mobility.

Stark broadening of the H_α band shown in Fig. 5 was used to estimate the electron densities shown in Fig. 6 [13]. The electron density with argon carrier gas decreased significantly, over 50%, as the pulse frequency was increased from 1 to 30 kHz. No change was seen when frequency was increased further to 60 kHz. This decrease is likely due to the decrease in energy per pulse.

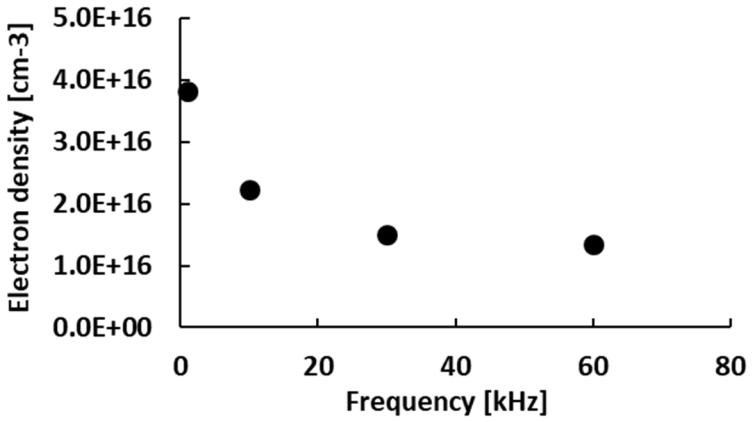

Fig. 6. Electron density as a function of pulse frequency for argon carrier gas.

3.2 Chemical analysis

Production rates of H_2O_2 measured in the liquid samples and H_2 and O_2 measured in the gas phase are shown in Fig. 7 for both argon and helium as functions of pulse frequency. All chemical species show an increase in production rate with pulse frequency. H_2O_2 and H_2 production rates were higher with helium than argon which is consistent with our previous work [11]. The increase in production rates of H_2 and O_2 are approximately linear with pulse frequency in helium, and H_2 only starts to level off slightly at high frequency in argon. These linear trends indicate that production of these species is not significantly affected by successive plasma channels. In contrast, the trend of H_2O_2 production rate with pulse frequency clearly deviates from linearity. This deviation can be partially attributed to the decrease in energy per pulse. However, the differences in the trend of production rates for the gas and liquid phase species also suggests that more degradation of formed H_2O_2 occurs at higher frequencies due to the significantly longer residence time of the liquid as compared to the gas phase, i.e., 150 ms to 2.5 ms, respectively [8]. Previous work has shown that hydroxyl radicals from the plasma can lead to degradation of formed chemical species [9, 10]. It should also be noted that some minimal warming of the liquid effluent was observed at the highest pulse frequencies investigated (highest discharge powers), however the change was not quantified in this study. It is possible this could lead to some thermal degradation of the formed H_2O_2 which could contribute to the drop in H_2O_2 energy yield at high pulse frequencies. In future work we plan to add a thermocouple to the system to assess the temperature of the effluent to further assess this hypothesis.

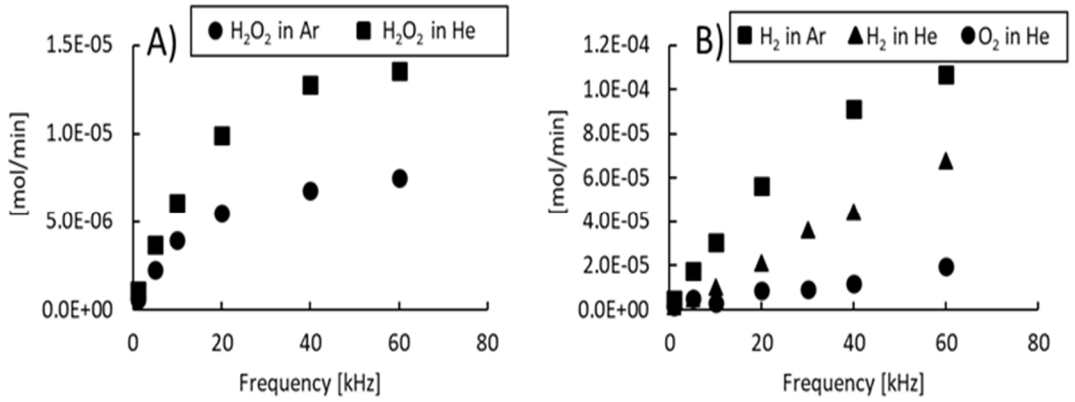

Fig. 7. A) Production rate of H_2O_2 for both argon and helium carrier gasses. B) Production rate of H_2 for both argon and helium carrier gasses as well as O_2 for helium.

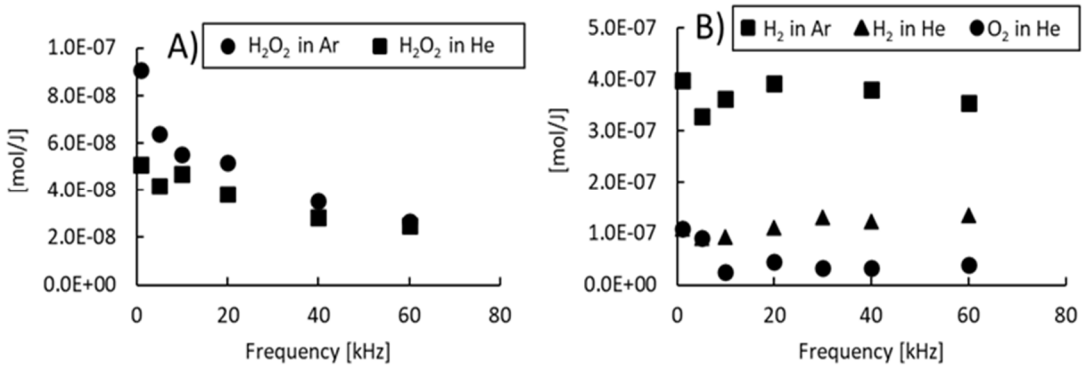

Fig. 8. A) Energy yield of H_2O_2 for argon and helium carrier gasses. B) Energy yield of H_2 for argon and helium carrier gasses and O_2 for helium.

The energy yields for H_2O_2, H_2, and O_2 as functions of pulse frequency are shown in Fig. 8. For H_2O_2, the energy yield decreases significantly with increasing pulse frequency. This provides further evidence that there must be some other reason for the drop in H_2O_2 production per pulse with increasing pulse frequency besides the decrease in energy per pulse. The energy yield would be constant as a function of frequency if the decrease in production rate was solely attributed to the drop in energy. In contrast, energy yields for the species measured

in the gas phase are relatively unaffected by pulse frequency. As suggested previously, this difference in the trends of gas phase verses liquid phase product generation indicates that the gas phase species are able to rapidly exit the reactor due to the short residence time of the gas phase, while products which are sequestered in the liquid have a higher likelihood of degradation by successive pulses due to the significantly longer residence time of the liquid phase. We currently do not have an explanation for the drop in the O_2 energy yield between 1−10 kHz. It is possible there could be a link to the electron density dropping significantly between 1 and 10 kHz, however this is highly speculative. It should be mentioned that while the error associated with the O_2 production rate and power were rather low (error bars within the markers), the error for O_2 was highest at the lowest pulse frequencies investigated (low O_2 concentrations). Thus, it is possible the decrease is simply being magnified by experimental error.

Table 1. Comparison of the relative production rates for H_2O_2, H_2, and O_2 as a function of pulse frequency for helium, A, and argon, B.

A) Helium				B) Argon			
Frequency (kHz)	H_2O_2	H_2	O_2	Frequency (kHz)	H_2O_2	H_2	O_2
60	1.0	5.0	1.5	60	1.0	14.2	N/A
40	1.0	3.5	0.9	40	1.0	13.4	N/A
20	1.0	2.2	0.9	20	1.0	10.2	N/A
10	1.0	1.7	0.5	10	1.0	7.7	N/A
5	1.0	1.4	1.4	5	1.0	7.9	N/A
1	1.0	1.2	1.2	1	1.0	7.8	N/A

Table 2. Comparison of the relative production rates for H_2O_2, H_2, and O_2 in other plasma systems.

Discharge type	H_2O_2	H_2	O_2	Ref.
Gliding are	1.0	4.0	N/A	[6]
Underwater discharge	1.0	2.0	0.4	[14]
Underwater discharge	1.0	2.0	0.5	[23]
Underwater discharge	1.0	1.6	0.4	[23]

Table 1 provides the relative production rates for H_2O_2, H_2, and O_2 formation for both argon and helium carrier gasses as functions of pulse frequency. Table 2 shows the relative production rates of these species for other types of plasma discharges including a gas/liquid gliding arc discharge with argon carrier and water spray operated with a 250 Hz microsecond pulse (1.5 W), an underwater discharge operated by a 60 Hz rotating spark gap (37–72 W), and a mathematical model based on the latter system. When the rate of formation of H_2O_2 to H_2 is compared for argon and helium in this work, the ratio of H_2 to H_2O_2 was significantly higher for argon than for helium at all pulse frequencies. For both carrier gases, this ratio decreased with decreasing pulse frequency, and this is mostly due to the drop in H_2O_2 energy yield with frequency since the energy yields of H_2 and O_2 are relative constant with changing frequency (Figure 8 B). In comparison to other types of plasma discharges, gliding arc in the gas phase with water spray and pulsed corona underwater, the results are similar for the low frequency case with helium carrier gas in the present reactor. In contract, for the case of argon in this work, the ratio of H_2 to H_2O_2 was significantly higher. The decrease in the ratio of H_2O_2 to H_2 with increasing pulse frequency provides further evidence of enhanced degradation with increasing pulse frequency. However, as in the previous work, further modeling will be needed to utilize these results in assessing the reaction pathways for the formation and degradation of these species [23, 24].

4. Conclusion

Analysis of the gas and liquid phase products produced when nanosecond filamentary non-thermal plasma channels propagate along a flowing liquid water film with an inert carrier gas show significant production of H_2O_2 in the liquid phase and H_2 and O_2 in the gas phase. These chemical species are generated through water dissociation by the plasma. The energy yield for H_2O_2 decreased as the pulse frequency of the discharge was increased while it remained relatively unchanged for the gas phase products, H_2 and O_2. This result suggests that gas phase species are less likely to be degraded than liquid products by successive plasma channels as the period between pulses decreases due to the significantly shorter residence time of the gas phase. Future experiments are planned to further investigate how the plasma properties such as electron density and plasma gas temperature affect the production and degradation of H_2O_2, H_2, and O_2.

Acknowledgment

Czech Fulbright Commission, Florida State University, US National Science Foundation NSF CBET-1702166, MEYS OP VVV IPP – Mobility CZ.02.2.69/0.0/0.0/16_027/0008354 and GACR 19-25026S.

References

[1] Bruggeman P. J., Kushner M. J., Locke B. R., Gardeniers J. G. E., Graham W. G., Graves D. B., Hofman-Caris R. C. H. M., Maric D., Reid J. P., Ceriani E., Rivas D. F., Foster J. E., Garrick S. C., Gorbanev Y., Hamaguchi S., Iza F., Jablonowski H., Klimova E., Kolb J., Krcma F., Lukes P., Machala Z., Marinov I., Mariotti D., Thagard S. M., Minakata D., Neyts E. C., Pawlat J., Petrovic Z. L., Pflieger R., Reuter S., Schram D. C., Schroter S., Shiraiwa M., Tarabova B., Tsai P. A., Verlet J. R. R., Woedtke T. von, Wilson K. R., Yasui K., and Zvereva G., Plasma-liquid interactions: a review and roadmap, *Plasma Sources Sci. Technol*., Vol. 25 (5), pp. 053002, 2016.

[2] Weltmann K.D., Kolb J. F., Holub M., Uhrlandt D., Simek M., Ostrikov K., Hamaguchi S., Cvelbar U., Cernak M., Locke B., Fridman A., Favia P., and Becker K., The future for plasma science and technology, *Plasma Process. Polym*., Vol. 16 (1), pp. 1800118, Jan, 2019.

[3] Brandenburg R., Bogaerts A., Bongers W., Fridman A., Fridman G., Locke B. R., Miller V., Reuter S., Schiorlin M., Verreycken T., and Ostrikov K., White paper on the future of plasma science in environment, for gas conversion and agriculture, *Plasma Process. Polym.*, Vol. 16 (1), pp. 1700238, 2019.

[4] Jiang B., Zheng J., Qiu S., Wu M., Zhang Q., Yan Z., and Xue Q., Review on electrical discharge plasma technology for wastewater remediation, *Chem. Eng. J*., Vol. 236, pp. 348–368, Jan 15, 2014.

[5] Locke B. R., and Shih K. Y., Review of the methods to form hydrogen peroxide in electrical discharge plasma with liquid water, *Plasma Sources Sci. Technol*., Vol. 20, pp. 034006, Jun., 2011.

[6] Burlica R., Shih K. Y., and Locke B. R., Formation of H_2 and H_2O_2 in a water-spray gliding arc nonthermal plasma reactor, *Ind. Eng. Chem. Res*., Vol. 49 (14), pp. 6342–6349, Sep. 18, 2010.

[7] Wandell R. J., and Locke B. R., Low-power pulsed plasma discharge in a water film reactor, *IEEE Trans. Plasma Sci.*, Vol. 42 (10), pp. 2634–2635, 2014.

[8] Wandell R. J., Wang H. H., Tachibana K., Makled B., and Locke B. R., Nanosecond pulsed plasma discharge over a flowing water film: Characterization of hydrodynamics, electrical, and plasma properties and their effect on hydrogen peroxide generation, *Plasma Process. Polym*., Vol. 15 (6), pp. 1800008, Jun, 2018.

[9] Xiong Y., Zhang Q., Wandell R. J., Bresch S., Wang H., Locke B. R., and Tang Y., Synergistic 1,4-dioxane removal by non- thermal plasma followed by biodegradation, *Chem. Eng. J*., Vol. 361, pp. 519–527, Apr 1, 2019.

[10] Hsieh K., Wang H. J., and Locke B. R., Analysis of a gas-liquid film plasma reactor for organic compound oxidation, *J. Hazard. Mater*., Vol. 317, pp. 188–197, Nov, 2016.

[11] Wang H. H., Wandell R. J., and Locke B. R., The influence of carrier gas on plasma properties and hydrogen peroxide production in a nanosecond pulsed plasma discharge generated in a water-film plasma reactor, *J. Phys. D: Appl. Phys*., Vol. 51 (9), pp. 094002, Mar, 2018.

[12] Hsieh K. C., Wandell R. J., Bresch S., and Locke B. R., Analysis of hydroxyl radical formation in a gas-liquid electrical discharge plasma reactor utilizing liquid and gaseous radical scavengers, *Plasma Process. Polym.*, Vol. 14 (8), pp. 1600171, Aug, 2017.

[13] Wang H. H., Wandell R. J., Tachibana K., Vorac J., and Locke B. R., The influence of liquid conductivity on electrical breakdown and hydrogen peroxide production in a nanosecond pulsed plasma discharge generated in a water-film plasma reactor, *J. Phys. D: Appl. Phys*., Vol. 52 (7), pp. 075201, Feb, 2019.

[14] Kirkpatrick M. J., and Locke B. R., Hydrogen, oxygen, and hydrogen peroxide formation in aqueous phase pulsed corona electrical discharge, Ind. Eng. Chem. Res., Vol. 44 (12), pp. 4243–4248, Jun, 2005.

[15] Wandell R. J., Wang H., Bulusu R. K., Gallan R. O., and Locke B. R., Formation of nitrogen oxides by nanosecond pulsed plasma discharges in gas–liquid reactors, *Plasma Chem. Plasma Process*., Vol. 39, pp. 643–666, 2019.
[16] Nikiforov A. Y., Leys C., Gonzalez M. A., and Walsh J. L., Electron density measurement in atmospheric pressure plasma jets: Stark broadening of hydrogenated and non-hydrogenated lines, *Plasma Sources Sci. Technol*., Vol. 24 (3), pp. 034001, May, 2015.
[17] Zhu X. M., Walsh J. L., Chen W. C., and Pu Y. K., Measurement of the temporal evolution of electron density in a nanosecond pulsed argon microplasma: using both Stark broadening and an OES line-ratio method, *J. Phys. D: Appl. Phys.*, Vol. 45 (29), pp. 295201, Jul, 2012.
[18] Eisenberg G. M., Colorimetric determination of hydrogen peroxide, *Ind. Eng. Chem. Anal. Ed*., Vol. 15 (5), pp. 327–328, 1943.
[19] Moon S. Y., Han J. W., and Choe W., Control of radio-frequency atmospheric pressure argon plasma characteristics by helium gas mixing, *Phys. Plasmas*, Vol. 13 (1), pp. 013504, Jan, 2006.
[20] Schroter S., Pothiraja R., Awakowicz P., Bibinov N., Boke M., Niermann B., and Winter J., Time-resolved characterization of a filamentary argon discharge at atmospheric pressure in a capillary using emission and absorption spectroscopy, *J. Phys. D: Appl. Phys.*, Vol. 46 (46), pp. 464009, Nov, 2013.
[21] Burm K., Calculation of the Townsend discharge coefficients and the Paschen curve coefficients, *Contrib. Plasma Phys.*, Vol. 47 (3), pp. 177-182, 2007.
[22] Shao T., Sun G. S., Yan P., Wang J., Yuan W. Q., Sun Y. H., and Zhang S. C., An experimental investigation of repetitive nanosecond-pulse breakdown in air, *J. Phys. D: Appl. Phys.*, Vol. 39 (10), pp. 2192–2197, May, 2006.
[23] Mededovic S., and Locke B. R., Primary chemical reactions in pulsed electrical discharge channels in water (Corrigendum), *J. Phys. D: Appl. Phys.*, Vol. 42 (4), pp. 049801, Feb, 2009.
[24] Mededovic S., and Locke B. R., Primary chemical reactions in pulsed electrical discharge channels in water, *J. Phys. D: Appl. Phys.*, Vol. 40 (24), pp. 7734–7746, Dec, 2007.